



Disease type detection in lung and colon cancer images using the complement approach of inefficient sets

Mesut Togaçar

Department of Computer Technology, Technical Sciences Vocational School, Firat University Elazig, Turkey



ARTICLE INFO

Keywords:

Histopathological images
Complement in sets
Metaheuristic optimization
Deep learning

ABSTRACT

Lung and colon cancers are deadly diseases that can develop simultaneously in organs and adversely affect human life in some special cases. Although the frequency of simultaneous occurrence of these two types of cancer is unlikely, there is a high probability of metastasis between the two organs if not diagnosed early. Traditionally, specialists have to go through a lengthy and complicated process to examine histopathological images and diagnose cancer cases; yet, it is now possible to achieve this process faster with the available technological possibilities. In this study, artificial intelligence-supported model and optimization methods were used to realize the classification of lung and colon cancers' histopathological images. The used dataset has five classes of histopathological images consisting of two colon cancer classes and three lung cancer classes. In the proposed approach, the image classes were trained from scratch with the DarkNet-19 model, which is one of the deep learning models. In the feature set extracted from the DarkNet-19 model, selection of the inefficient features was performed by using Equilibrium and Manta Ray Foraging optimization algorithms. Then, the set containing the inefficient features was distinguished from the rest of the set features, creating an efficient feature set (complementary rule insets). The efficient features obtained by the two used optimization algorithms were combined and classified with the Support Vector Machine (SVM) method. The overall accuracy rate obtained in the classification process was 99.69%. Based on the outcomes of this study, it has been observed that using the complementary method together with some optimization methods improved the classification performance of the dataset.

1. Introduction

Malignant cells, which are formed by abnormal division and reproduction of certain cells in an organ or tissue, are called cancer [1]. A tumor is a mass or lump of tissue that can appear on almost any part of the body. Not every tumor is a cancer cell. Cells that grow slowly in tumor cells and do not harm the surrounding tissues in the region where they are formed are called benign. These cells are not considered cancer. On the other hand, cells that grow rapidly and abnormally and that can spread to the surrounding tissues are malignant tumors. Malignant tumors are cancer-causing cells [2]. According to a statistical study conducted in America, it is estimated that lung and colon cancers will be in the top three among the most common cancer types in 2020. In addition, the research predicted that in 2020, among all cancer cases in America, the highest death rates will be seen in lung and colon cancers patients [3]. Although lung cancer cases are not frequent, they can be seen simultaneously with colon cancer. The rate of the simultaneous occurrence of these two types of cancer in the conducted study is

approximately 17%. Apart from this, in the absence of an early diagnosis, the metastasis of cancer cells between the two organs is quite high. It is known that smoking has a negative effect on the formation of lung cancer and it is said to be caused by an unconscious diet in the formation of colon cancer [4].

In the last few decades, extensive deployment of technological opportunities in biomedical applications for both diagnosis and treatment processes of cancer types. The decision-making process of specialists can take a long time in the diagnosis process of cancer cases [5,6]. In this case, artificial intelligence technologies, which provide the opportunity to make decisions by examining data more quickly, have recently become known. In this study, the data consisting of histopathological images of lung and colon cancers were examined. Cancer types are determined by using a deep learning model, which is the sub-branch of artificial intelligence, with optimization methods [7,8]. Many studies conducted using deep learning models in the detection of lung and colon cancers are available in the literature. For instance, Wang et al. [9] performed the classification of lung cancer pathology images with

E-mail address: mtogacar@firat.edu.tr.

Convolution Neural Network (CNN) based on the cell segmentation method. They used the Softmax activation function in the last layer of the CNN model for the classification process. Using the Region of Interest (ROI) technique as preprocessing step to their data, they focused on the area of the cells with the relevant tumors. The classification success achieved in the three-class image set was 90.1%. Teramoto et al. [10] managed to detect histopathological images of three classes of lung cancer with a deep learning model. They used the augmentation approach and deployed rotate, flip, and filter techniques for each image. Then they performed the classification process with the deep CNN model they designed. Their classification success was about 70%. Wei et al. [11] performed the classification of six-class lung cancer histopathological images by CNNs, where they used ResNet models in their study. They used ImageNet and COCO image-based pre-trained approaches in ResNet models. Before model training, the input data was passed through preprocessing step with the augmentation technique. The classification F-score success in their study was 90.4%. Shapcott et al. [12] performed their classifications with a deep learning approach by using histopathological images of colon cancer. The dataset consists of four classes. The cell identification algorithm for cell patches was applied to each image. Here, they divided the images into specific sizes by segmenting. They performed the classification process via cell patches defined by the used CNN model. The correlation accuracy rates they obtained were between 90% and 96.9%. Gessert et al. [13] performed the classification process with transfer learning-based CNN models using colon cancer microscopic images. A dataset consisting of benign and malignant images was used in their study. They performed dataset training with models such as Inception, VGG, and DenseNet. With the DenseNet model, they achieved the best classification success, where they obtained a classification accuracy rate of 91.2% using this model. Vuong et al. [14] suggested a multi-purpose learning approach to analyze digitized images of pathology. In their study, a dataset of pathology images consisted of four classes was used. They set the input data to the model as 800×800 pixels and used the DenseNet-121 model for dataset training. The classification accuracy rate they obtained was 85.91%.

In this study, an artificial intelligence-based approach that detects cancer types using histopathological images is proposed. In the proposed approach, it is aimed to select inefficient features by applying meta-heuristic optimization algorithms to feature sets extracted from images. Inefficient features are known as numeric values that have low distinctiveness in correctly recognizing the label class of each image. In the proposed approach, it is targeted to successfully classify cancer types by applying the mathematical “complement” rule to obtain efficient features [15,16].

Other sections are organized as follows: Material and methods are presented in Section 2, experimental analyzes and results are reported in Section 3, a discussion of the experimental analyzes and a comparison with other studies is presented in Section 4, and the conclusions and remarks are given in Section 5.

2. Material and methods

2.1. Lung and colon cancer dataset

The dataset consists of five classes and contains a total of 25,000 histopathological images, 5000 images from each class. The dataset images are of JPEG extension consisting of lung and colon tissues. The used lung tissue images consist of three classes, which are lung benign tissue, lung adenocarcinoma, and lung squamous cell carcinoma. Besides, the colon texture consists of two image classes, which are colon adenocarcinoma and colon benign tissue. Each image in the dataset has a resolution of 768×768 pixels. The images were checked and presented by radiologists and specialists. All images are de-identified, according to the Health Insurance Portability and Accountability Act compliant, and are freely available for download to researchers [17,18].

Malignant tumors make up the classes that cause lung or colon cancer depending on the type of tissue. Sample images of the five classes that make up the dataset are shown in Fig. 1.

In this study, 25,000 images were used in all steps of the experiment. 30% of the dataset was used as test data, and 70% was allocated as training data. In addition, cross-validation was applied at some steps of the experiment, and the cross-validation variable was chosen five ($k = 5$).

2.2. DarkNet-19

DarkNet-19 is a deep learning model based on the YOLO object detection model. The DarkNet-19 architectural structure contains nineteen convolutional layers and five pooling layers [19]. They provide the activation maps by circulating the input data with the convolutional layers and the selected filters. The activation maps contain the features obtained with filters. The pooling layer combines the outputs of neurons from one layer into a single neuron output to transfer the output to the next layer, thereby reducing the size of the data [20]. The DarkNet-19 model uses 3×3 filters after convolutional layers, similar to the VGG models, and the number of channels is doubled. In addition, the DarkNet-19 model uses batch normalization to speed up convergence, stabilize the training process and streamline the functioning of the model [19]. The preferred parameter values of the DarkNet-19 model for this study are given in Table 1.

The reasons for choosing DarkNet-19 in this study are as follows: the DarkNet-19 model has a state-of-the-art architecture designed to detect real-time objects [21]; therefore, it plays a more active role in computer-aided systems designed for disease detection in real life. Another reason is that each image resolution in the dataset consists of 768×768 pixels, and the input size of the DarkNet-19 model is 256×256 . Therefore, the resolution (width/height ratio) of each image can be given as an input to the DarkNet-19 model without loss.

For this study, the DarkNet-19 model was trained from scratch using MATLAB software. The main reason for training the DarkNet-19 model from scratch was to obtain a percentile that could contribute to the overall accuracy success of the proposed approach. The hardware resources used for the experimental analysis were also sufficient to train the DarkNet-19 model from scratch. In the last layer of DarkNet-19, the SVM method is used for classification. In the process of determining the classification method, Softmax was compared with the Nearest Neighbor, Random Forest, and Discriminant Analysis methods, and it was preferred in this study because the SVM method gave the most efficient classification result. This method was preferred because it is widely used in the solution of remote pattern recognition and classification problems and successfully executes multiple classification processes [22–24]. Other selected parameters for the DarkNet-19 model, i.e. learning rate 10^{-5} , epoch value 16, and mini-batch value 128 were selected. In addition, the feature sets used in the experimental analysis were obtained from the Avg1 layer of the DarkNet-19 model.

2.3. Support Vector Machine

SVM method is a machine learning algorithm preferred in regression and classification processes in deep learning methods. It can successfully perform binary classification or multiple classification processes in classification methods. In this method, the features obtained by the CNN model are divided into classes with hyperplanes. In multiple classes, the SVM method performs voting for features that are in the positive or negative region of the hyperplane. As a result of the voting, each feature is transferred to the class in which it received high votes. The overall design of the multi-class SVM method is shown in Fig. 2, and the general equations used in the classification process are specified in Eqs. (1)–(3). Here, X and Y represent the coordinate points of the features in the hyperplane. W parameter represents margin width and b parameter represents bias value [25,26].

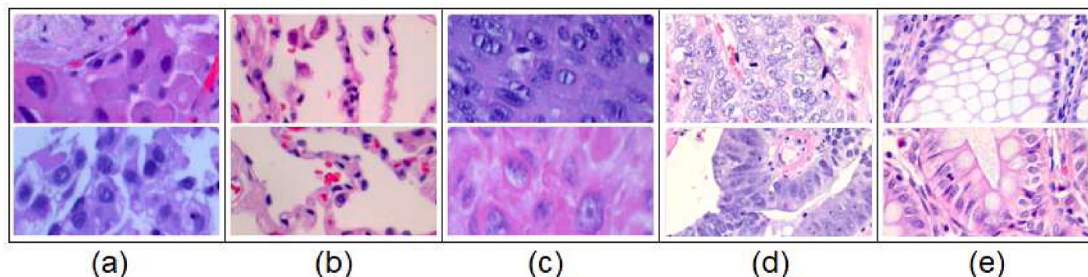


Fig. 1. Lung histopathological sample images: (a) adenocarcinoma, (b) benign tissue, (c) squamous cell carcinoma and colon histopathological sample images, (d) adenocarcinoma, (e) benign tissue.

Table 1
Parameters and values of the DarkNet-19 model used in this study.

Layers	Filters	Size/Stride	Output
Convolutional	32	3×3	256×256
Max pool		$2 \times 2/2$	128×128
Convolutional	64	3×3	128×128
Max pool		$2 \times 2/2$	64×64
Convolutional	128	3×3	64×64
Convolutional	64	1×1	64×64
Convolutional	128	3×3	64×64
Max pool		$2 \times 2/2$	32×32
Convolutional	256	3×3	32×32
Convolutional	128	1×1	32×32
Convolutional	256	3×3	32×32
Max pool		$2 \times 2/2$	16×16
Convolutional	512	3×3	16×16
Convolutional	256	1×1	16×16
Convolutional	512	3×3	16×16
Convolutional	256	1×1	16×16
Convolutional	512	3×3	16×16
Max pool		$2 \times 2/2$	8×8
Convolutional	1024	3×3	8×8
Convolutional	512	1×1	8×8
Convolutional	1024	3×3	8×8
Convolutional	512	1×1	8×8
Convolutional	1024	3×3	8×8
Convolutional	1000	1×1	8×8
Avg1		Global	1000
Linear SVM			

There are several types of SVM applications that have a strong potential in solving data analysis problems encountered in daily life. For this study, the SVM types (cubic, linear, quadratic, etc.) were tested, and linear SVM was used in all experimental stages, as it performed best in the early stages of the experiment. The preferred parameter values of the linear SVM method for this study, namely the kernel scale parameter, which was automatically selected, and the box constraint level parameter value, which was selected, and the multi-class method parameter, which was selected one-to-one.

$$u = w \cdot x - b \quad (1)$$

$$\frac{1}{2} \|w\|^2 \quad (2)$$

$$y_i(w \cdot x_i - b) \geq 1, \forall i \quad (3)$$

2.4. Manta Ray Foraging Optimization algorithm

Optimization methods are used to make engineering approaches easier in solving real problems in the world. Manta Ray Foraging Optimization (MRFO) is a metaheuristic method inspired by the intelligent behavior of manta rays. Manta Ray is one of the biggest sea creatures. These creatures generally feed on plankton produced from microscopic animals. Planktons are heterogeneously dispersed in the sea and Manta Rays travel in groups to identify the places where planktons are predominant with the baiting tactic they have developed. The foraging strategy takes place in three ways: chain foraging where fifty and more Manta Rays are lined up one after the other, looking for plankton nutrients by forming a smooth line. Planktons that are overlooked in this way are seen by the Manta Rays at the end of the line. Manta Rays, which transfer the most plankton to their gills, can increase their food rewards in this way. Cyclone foraging, which takes place when the plankton food is dense. The tail ends of the Manta Rays form a spiral maximum point in the eye of the cyclone. Thus, they allow the water filtered by the tail tips to move towards the surface and easily catch the plankton nutrients as the Manta Rays keep their mouth open. When the Swarm of Manta Ray finds a plankton food source with a somersault foraging, they roam around this food source and roll over. They perform this somersault movement in the local area and a cyclical manner. Thus, they optimize the intake of plankton nutrients more easily [27].

The first operation of the MRFO randomly determines a location to start optimization according to Eq. (4). In this equation, the variable $r(\cdot)$ represents a random number between 0 and 1, and Lb and Hb parameters represent the maximum and minimum limits of the problem control values. X also gives location information. Manta Rays updates according to Eq. (5) to find the best foods. At the end of this step, the new positions of the Manta Rays are updated around the best position using the formula in Eq. (6). The parameters r_2 and r_3 in Eq. (5) and Eq. (6) take a random number value between 0 and 1. The SF parameter is the somersault factor. While the X_{best} parameter gives the position of the best nutrient with high concentration; λ parameter, on the other hand,

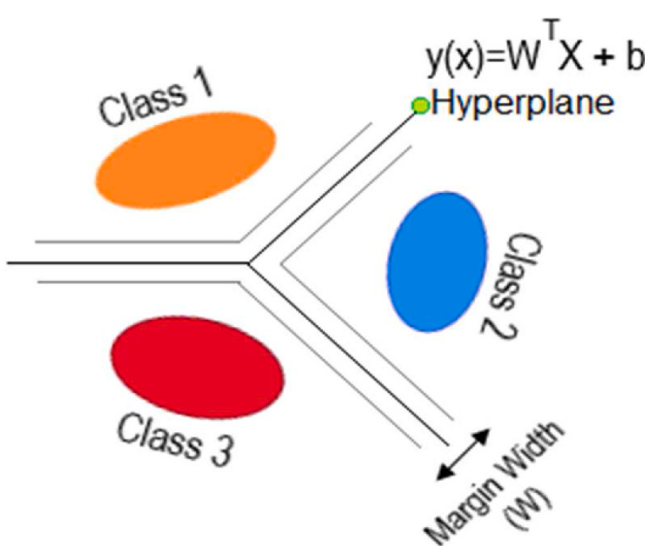


Fig. 2. The general design of the multi-class SVM method.

represents an adjustable amount of value in the water region of the Manta Rays [28].

$$X_{ij}(\cdot) = Lb_{ij} + r(\cdot) x (Hb_{ij} - Lb_{ij}) \quad (4)$$

$$X_{ij}(t+1) = X_{ij}(t) + (X_{bestj}(t) - X_{ij}(t))x(r(\cdot) - \lambda) \quad (5)$$

$$X_{ij}(t+1) = X_{ij}(t) + SF x (r_2 x X_{bestj} - r_3 x X_{ij}(t)) \quad (6)$$

The detailed information on the three foraging strategies used by MRFO is as follows chain foraging performs the process of finding food by mimicking it. If there is a lost prey in this chain, it systematically uses the last manta ray to find it. In chain foraging, X_k is represented as the seeker and performs operations according to Eq. (7) and Eq. (8). The X_k agent is updated with each iteration (k). Here, the variable k represents its position, the time t , and the variable r the random vector that can take values in the range of $[0, 1]$. Also, high concentration plankton is represented by X_{best}^t and the weight coefficient is represented by the variable α [29].

$$X_k^{t+1} = \begin{cases} X_k^t + r^*(X_{best}^t - X_k^t) + \alpha(X_{best}^t - X_k^t), & k = 1 \\ X_k^t + r^*(X_{k-1}^t - X_k^t) + \alpha(X_{best}^t - X_k^t), & k = 2, \dots, N \end{cases} \quad (7)$$

$$\alpha = 2 * r^* \sqrt{|\log(r)|} \quad (8)$$

The total amount of prey is important in the cyclone foraging strategy, and when this amount is caught, the cyclone foraging strategy is performed. The head is paired with the tail of the manta ray, and a spiral is created to form an edge in the eye of a cyclone. The X_k tool update in cyclone search occurs according to Eq. (9). Weight coefficient is represented by variable β and calculated according to Eq. (10) [29].

$$X_k^{t+1} = \begin{cases} X_{best}^t + r^*(X_{best}^t - X_k^t) + \beta(X_{best}^t - X_k^t), & k = 1 \\ X_{best}^t + r^*(X_{k-1}^t - X_k^t) + \beta(X_{best}^t - X_k^t), & k = 2, \dots, N \end{cases} \quad (9)$$

$$\beta = 2 * \exp\left(r * \frac{K_{max} - k + 1}{K_{max}}\right) * \sin(2\pi r) \quad (10)$$

In the somersault foraging strategy, the best hunting location is considered the target point. Each manta ray in the population examines around the determined target point and updates its position status in the search area relative to this target point. It performs this action with backward rotation and circular movements. It uses the mathematical formula in Eq. (11) when calculating this operation. In this equation, δ is represented as the somersault factor [29,30].

$$X_k^{t+1} = X_k^t + \delta^* (r_1 X_{best}^t - r_2 X_k^t) \quad (11)$$

In this study, the somersault foraging strategy was used for the MRFO algorithm. Also for the MRFO algorithm, the population size of 20 was selected, the maximum iteration parameter one was selected, and the best global value parameter of 250 was taken for the start.

2.5. Equilibrium Optimizer algorithm

Equilibrium Optimizer (EO) includes an algorithm that predicts both dynamic and equilibrium states inspired by control volume mass balance models. Each particle used for the position (concentration) in EO functions as a search agent. In this way, all values are updated, thus, they contribute to the improvement of the model. EO was developed with a physics-based approach. It is therefore considered in the third optimization class. It provides the basic physics for the protection of input, processed, and output data in a control volume with mass balance. Over time, this equilibrium will be balanced with the amount processed and the amount of output. The differential equation that accomplishes this is stated below. In Eq. (12), V denotes the control volume, C denotes the concentration in volume. It also represents the $V \frac{dC}{dt}$ mass change rate, and the input and output speed in the Q control

volume. Furthermore, it represents the rate of production (change) in the G control volume, and C_{eq} represents the concentration in the case of an equilibrium in which there is no generation within the control volume [31].

$$V \frac{dC}{dt} = QC_{eq} - QC + G \quad (12)$$

Eq. (12) can be rearranged like Eq. (13) to solve the Concentration (C), where t represents time.

$$\frac{dC}{\lambda C_{eq} - \lambda C + \frac{G}{V}} = dt \quad (13)$$

Here, λ represents the turnover rate. Consequently, the position (concentration) update for EO is performed according to Eq. (14).

$$C = C_{eq} + (C_o - C_{eq}) F + \frac{G}{\lambda V} (1 - F) \quad (14)$$

The value of the variable F in Eq. (14) is calculated according to Eq. (15). It is used in Eq. (14) to estimate the concentration or to calculate the average turnover rate.

$$F = \exp - \lambda(t - t_0) \quad (15)$$

This update in Eq. (14) is similar to the particle swarm optimization algorithm. In EO, the pool of populations is chosen randomly, similar to other meta-heuristics algorithms. So, there is no preliminary information about equilibrium state parameters for EO. These parameters are improved by updating weights and this process continues until the optimal balance is achieved [31]. For this study, the population size of 20 was selected, the maximum iteration parameter was set to one, the best global value parameter was taken for the start as 250, and the starting value of G parameter was selected as 0.5.

From the fitness function of feature selection, the value of the function can become optimal when the accuracy of the selected features is good. The purpose of the feature selection method is to select as few features as possible with high classification accuracy. The fitness function of the optimization algorithms used in this study was calculated according to Eq. (16). In this equation, $\gamma p(\text{Error})$ represents the error rate of the features selected by the classifier. The total number of features is represented by $|F_{sum}|$ and the currently selected number of features is represented by $|F_{selected}|$. The weight coefficients are represented by Ω and Ω' . Ω and Ω' are complementary to each other. In other words, it is calculated as " $\Omega = 1 - \Omega'$ " with connection equations, and these two variables take random values between 0 and 1. The Ω value of 0.85 was preferred for the MRFO algorithm used in the experimental analysis, and the Ω' value of 0.9 was preferred for the BO algorithm.

$$Function_{fitness} = \Omega \gamma p(\text{Error}) + \Omega' \frac{|F_{selected}|}{|F_{sum}|} \quad (16)$$

2.6. Complementary approach in sets

The set that covers all clusters is called the "Universal Set". All clusters are the subset of the universal set (E); that is, the universal set covers all subsets. The set of elements in other sets outside of a set is called the "complement of this set" [32,33]. The merged sets are a subset of the Universal Set, and the complement of the merged sets is shown in Fig. 3. Here, the unit U refers to the complement of the combined sets. In other words, it represents effective features outside the combination of the V and W sets. The set V represents ineffective features selected by EO and set W represents ineffective features selected by MRFO. Therefore, all effective and ineffective features are included in the universal set. The complementary status of Fig. 3 is given in Eq. (17).

$$U = \overline{(V \cup W)} = E - (V \cup W) \quad (17)$$

In this study, MRFO and EO methods [34] focused on inefficient feature selection by using feature sets obtained by the DarkNet-19

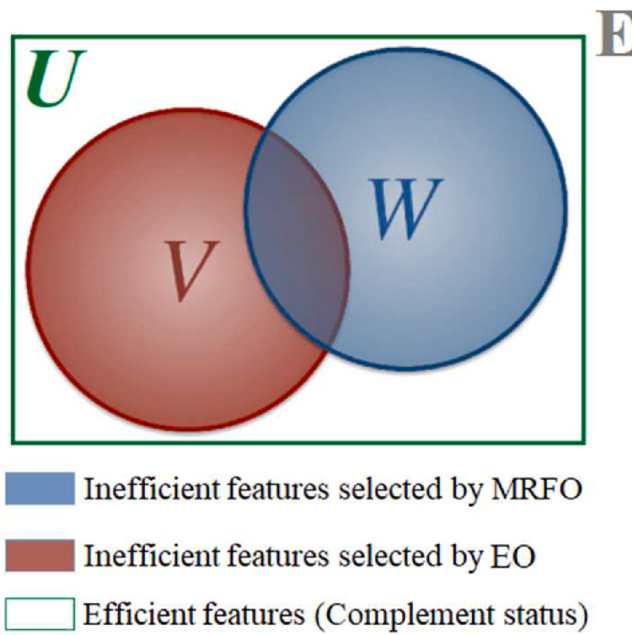


Fig. 3. Complementary state in combined sets using optimization methods.

model.

2.7. Proposed approach

The proposed approach has performed the classification of histopathological images that cause lung cancer and colon cancer. The contribution of the proposed approach to the literature is summarized in the following two items:

- To increase the efficiency of meta-heuristic optimization approaches in feature selection, instead of focusing on the selection of efficient features, the proposed approach focuses on detecting inefficient features that are out of the population. (Contrary to the approaches used in feature selection methods, a different perspective has been gained.)
- By applying the complement rule in sets, efficient feature sets were obtained by removing inefficient feature sets from all feature sets. (The case of using the mathematical rule in the proposed approach.)

The proposed approach consists of three parts. In the first part, it is aimed to obtain the feature set by training the used dataset by the Darknet-19 model from scratch. The layer with features is the Avg1 layer in the DarkNet-19 model, and it contains 1000 features [35]. Here, 'mat file' containing the features obtained after training of the model is used, and the operations are performed using column numbers representing the features of these files. The second part is aimed to focus on the selection of inefficient features by using 1000-feature set MRFO and EO algorithms that are extracted by the model. Here, the optimization algorithms are provided to be processed by holding the most inefficient feature left out of the population during each iteration by a variable. In this process, iterations of the two optimization algorithms were carried on until the number of inefficient features reached 250. Here, the selection of the number 250 (1/4 of 1000 features) was chosen randomly. The aim was to find and distinguish features that lower classification success from 1000 feature sets as much as possible. In the third part, the aim was to increase the classification performance with an effective feature set by distinguishing 500 (250 + 250) inefficient features obtained from two optimization algorithms from 1000 feature datasets (complement rule in the set). However, it is useful to state two points to be considered here. First, there are chances that the inefficient features

thrown out of the population by each optimization algorithm may be the same. Therefore, since the column numbers of inefficient features in 250 iterations may be the same, the total number of unrepeatable inefficient features may be below 250. Second, since the two optimization algorithms process the same dataset, the column numbers with inefficient features can be the same. In this case, the proposed approach provides us with less than 500 inefficient features. The overall design of the proposed approach is shown in Fig. 4. With the experimental analysis carried out in this study, the proposed approach has contributed to the improvement of classification performance.

3. Experimental results

MRFO and EO algorithms used in this study are designed in Python language. Optimization algorithms were compiled using Python 3.6 software and Jupiter Notebook interface [34]. The DarkNet-19 model was compiled using MATLAB (2020a) interface, and this interface was used in the classification process. The hardware features used for the analysis of the experiment are the processor is Intel © Xeon © Gold 6132 CPU @ 2.6 GHz, screen card is NVIDIA Quadro P6000 24 GB and memory card is 64 GB. The operating system is Windows 10 (64 bit). In the experiment of this study, confusion matrix and related metric parameters were used for measurement. The metric parameters used are as follows: sensitivity (Se), specificity (Sp), f-score (F-Score), precision (Pre), and accuracy (Acc). True Positive (TP), False Positive (FP), True Negative (TN), and False Negative (FN) parameters of the confusion matrix were used to calculate the metrics [36–38]. Metrics are calculated according to the following equations:

$$Se = \frac{TP}{TP + FN} \quad (18)$$

$$Sp = \frac{TN}{TN + FP} \quad (19)$$

$$Pre = \frac{TP}{TP + FP} \quad (20)$$

$$F - Scr = \frac{2xTP}{2xTP + FP + FN} \quad (21)$$

$$Acc = \frac{TP + TN}{TP + TN + FP + FN} \quad (22)$$

The parameter values of the DarkNet-19 model and meta-heuristic optimization algorithms used in the experimental analyzes of this study are usually the default values. The hardware resources used in the experimental analysis, the size of the dataset, the capacity of the feature sets caused some parameter values to change.

The experiment of this study consists of four steps. In the first step of the experiment, the dataset was trained from scratch by the DarkNet-19 model. The goal of this step was to determine the overall accuracy of the deep learning model and use the feature set for the next steps. Success and loss graphs related to training validation are shown in Fig. 5. Then, after the model was trained, it was classified using the SVM method. The overall accuracy rate obtained from the DarkNet-19 model as a result of the classification was 96.72%, and analysis results are given in Table 2. The confusion matrix of the overall accuracy success achieved in the first step is shown in Fig. 6.

In the second step, the 1000-feature set obtained from the Avg1 layer of the DarkNet-19 model was processed by MRFO and EO algorithms. Here, it was asked to select 250 inefficient features for each optimization algorithms. Therefore, 118 inefficient features were obtained that did not repeat with the MRFO algorithm. The overall accuracy rate of 118 inefficient features obtained by the SVM method was 96.57%. Then, the complement of inefficient features obtained with the MRFO algorithm was taken ($1000 - 118 = 782$). 782 efficient feature set was classified by SVM method and overall accuracy success was 98.21%. For the obtained

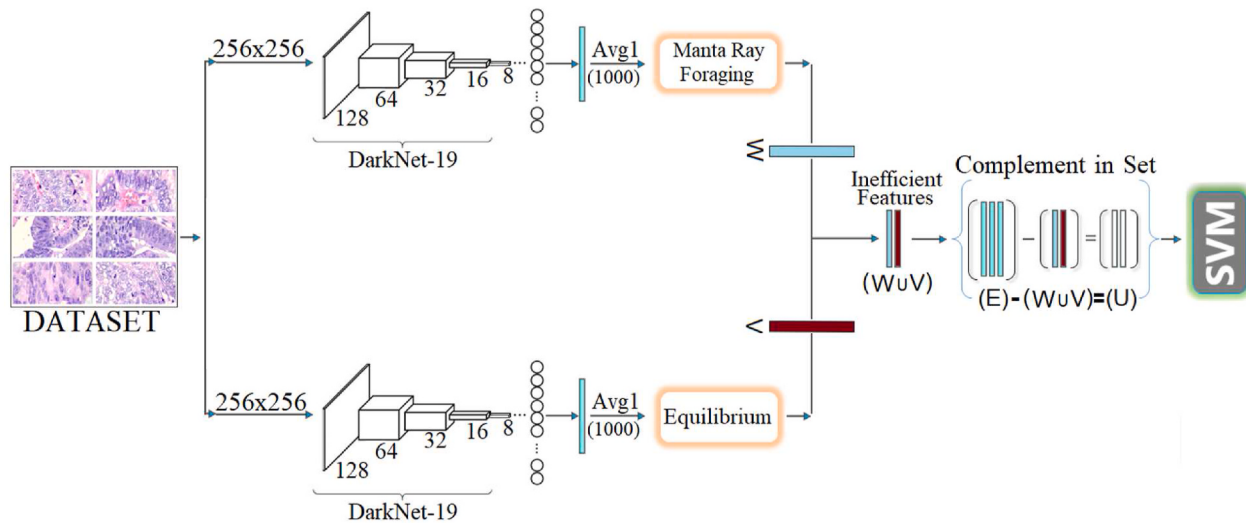


Fig. 4. The design of the proposed and implemented approach in the experiment of this study.

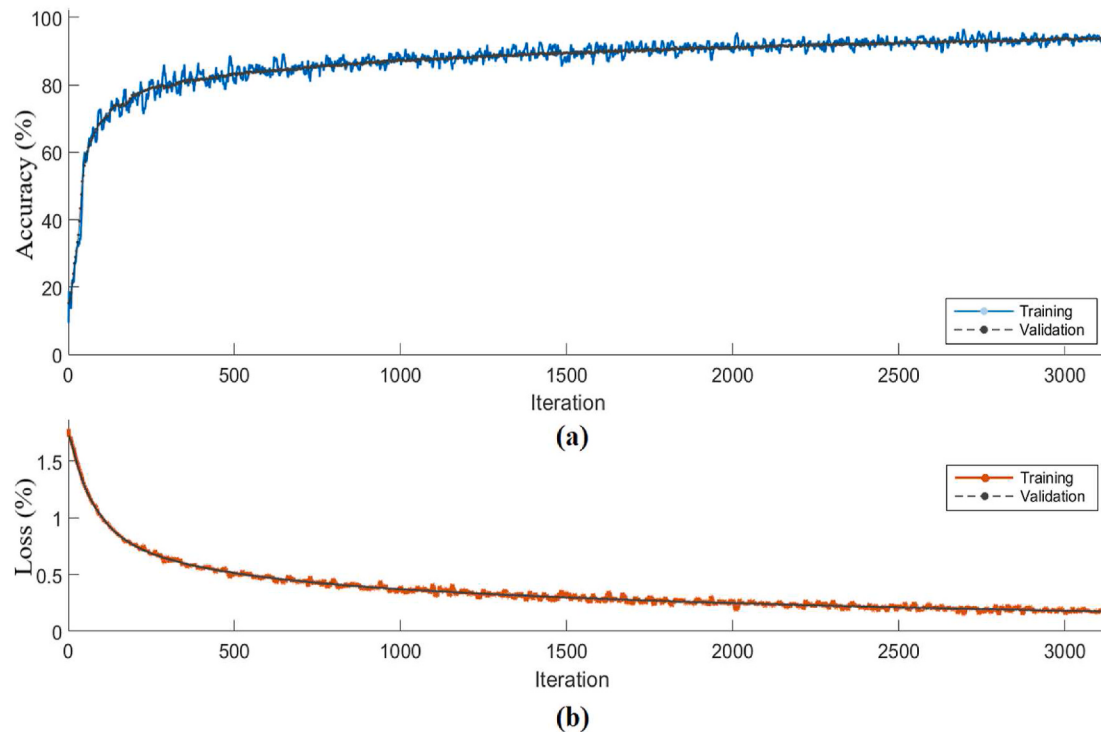


Fig. 5. Training and test graphics obtained by the DarkNet-19 model; (a) accuracy graphic, (b) loss graphic.

Table 2
Analysis results obtained by classification of DarkNet-19 model.

Model	Class	F-Scr. (%)	Se. (%)	Sp. (%)	Pre. (%)	Acc. (%)	Overall Acc. (%)
DarkNet-19	Colon adenocarcinoma	97.64	96.93	99.58	98.37	99.04	96.72
	Colon benign	97.84	98.60	99.24	97.11	99.11	
	Lung adenocarcinoma	93.97	93.66	98.56	94.29	97.57	
	Lung benign	99.70	99.93	99.86	99.46	99.87	
	Lung squamous cell carcinoma	94.40	94.46	98.56	94.34	97.73	

results to be valid, inefficient features (118 features) and efficient features (782 features) were cross-validated and re-classified with SVM. Accuracy success achieved with inefficient features was 96.91% and 97.95% obtained with efficient features. The confusion matrices

obtained by the MRFO algorithm are shown in Fig. 7. The analysis results obtained from the confusion matrices are given in Table 3 and Table 4 respectively. Similarly, 195 inefficient features were obtained which were not repeated with the EO algorithm. The accuracy rate of

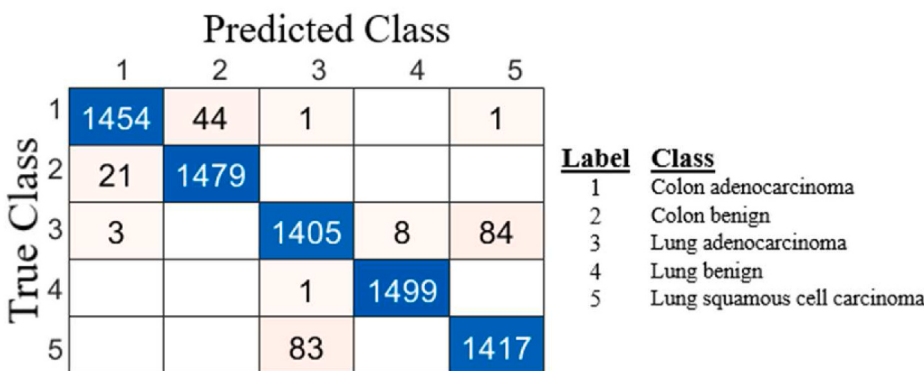


Fig. 6. The confusion matrix of the DarkNet-19 model.

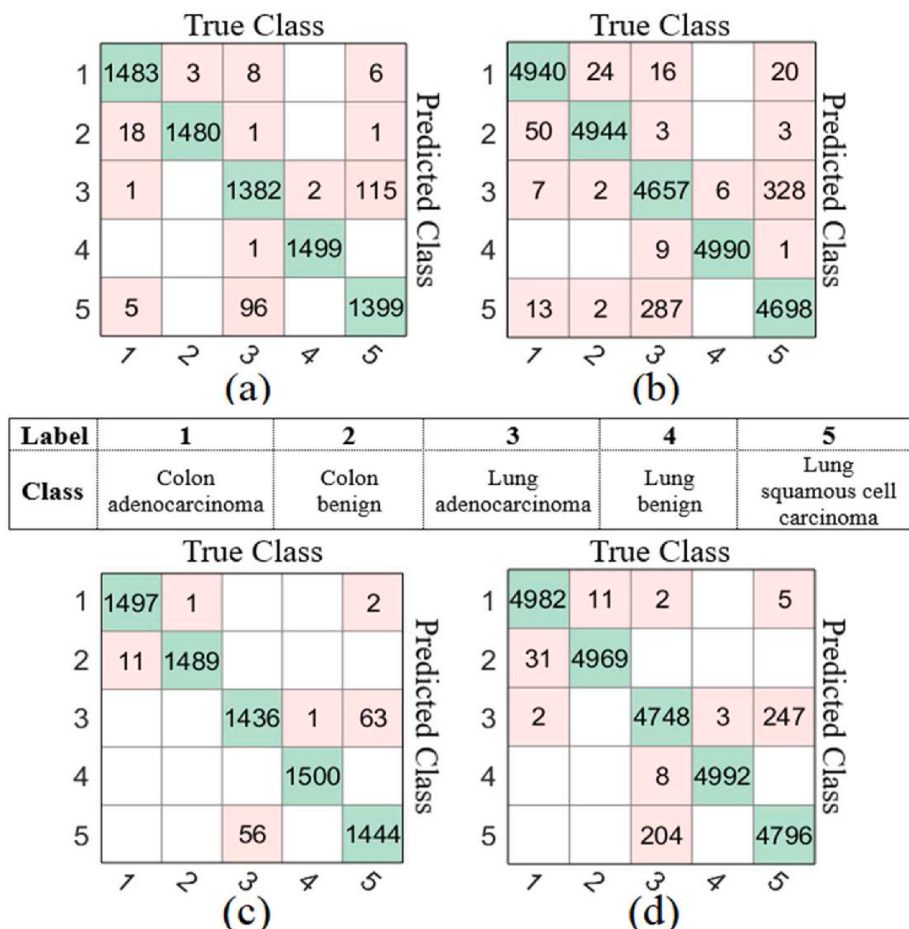


Fig. 7. The confusion matrices of the MRFO algorithm: (a) 30% test rate with inefficient feature set; (b) k fold value = 5 with inefficient feature set; (c) 30% test rate with efficient feature set; (d) k fold value = 5 with efficient feature set.

195 inefficient features obtained by the SVM method was 97.0%. Then, the complement of inefficient features obtained by the EO algorithm was taken ($1000 - 195 = 805$). The 805 effective feature set was classified according to the SVM method and the overall accuracy success was 98.0%. For the obtained results to be valid, inefficient features (195 features) and efficient features (805 features) were reclassified by the SVM method using cross-validation. Accuracy success achieved with inefficient features was 97.18%, and effective features were achieved as 97.94%. Confusion matrices obtained by the EO algorithm are shown in Fig. 8. The results of the analysis obtained from the confusion matrices are given in Table 5 and Table 6, respectively. As a result, it was

observed in this step that the two optimization algorithms contributed to the success of the proposed approach.

The third step is the step where the proposed approach is implemented. A new feature set was created by combining the inefficient features of the two optimization algorithms at this step. 118 inefficient features obtained by the MRFO algorithm and 195 inefficient features obtained by the EO algorithm were combined. During the merging of the two feature sets, the column numbers in both feature sets may also be the same. In this case, it is necessary to use the feature column numbers that intersect in the two sets once. In total, 270 unique inefficient features were obtained. The inefficient feature set (270 features) was

Table 3

Analysis results were obtained by the classification of the MRFO algorithm (inefficient features).

Class	Number Of Features	Test Rate	F-Scr. (%)	Se. (%)	Sp. (%)	Pre. (%)	Acc. (%)	Overall Acc. (%)
Colon adenocarcinoma	118	30%	98.63	98.86	99.58	98.40	99.43	96.57
Colon benign			99.22	98.66	99.94	99.79	99.68	
Lung adenocarcinoma			92.50	92.13	98.22	92.87	97	
Lung benign			99.90	99.93	99.96	99.86	99.95	
Lung squamous cell carcinoma			92.61	93.26	97.95	91.97	97.01	
Colon adenocarcinoma	k = 5	98.70	98.80	99.63	98.60	99.46		
Colon benign		99.15	98.88	99.85	99.43	99.65		
Lung adenocarcinoma		93.40	93.14	98.41	93.66	97.35		96.91
Lung benign		99.83	99.80	99.96	99.87	99.93		
Lung squamous cell carcinoma		93.49	93.96	98.22	93.02	97.37		

Table 4

Analysis results were obtained by the classification of the MRFO algorithm (efficient features).

Class	Number Of Features	Test Rate	F-Scr. (%)	Se. (%)	Sp. (%)	Pre. (%)	Acc. (%)	Overall Acc. (%)
Colon adenocarcinoma	782	30%	99.53	99.80	99.81	99.27	99.81	98.21
Colon benign			99.59	99.26	99.98	99.93	99.83	
Lung adenocarcinoma			95.98	95.73	99.06	96.24	98.39	
Lung benign			99.96	100	99.98	99.93	99.98	
Lung squamous cell carcinoma			95.97	96.26	98.91	95.69	98.38	
Colon adenocarcinoma	k = 5	99.49	99.64	99.83	99.34	99.79		97.95
Colon benign		99.57	99.38	99.94	99.77	99.82		
Lung adenocarcinoma		95.32	94.96	98.92	95.68	98.13		
Lung benign		99.88	99.84	99.98	99.93	99.95		
Lung squamous cell carcinoma		95.46	95.92	98.73	95.01	98.17		

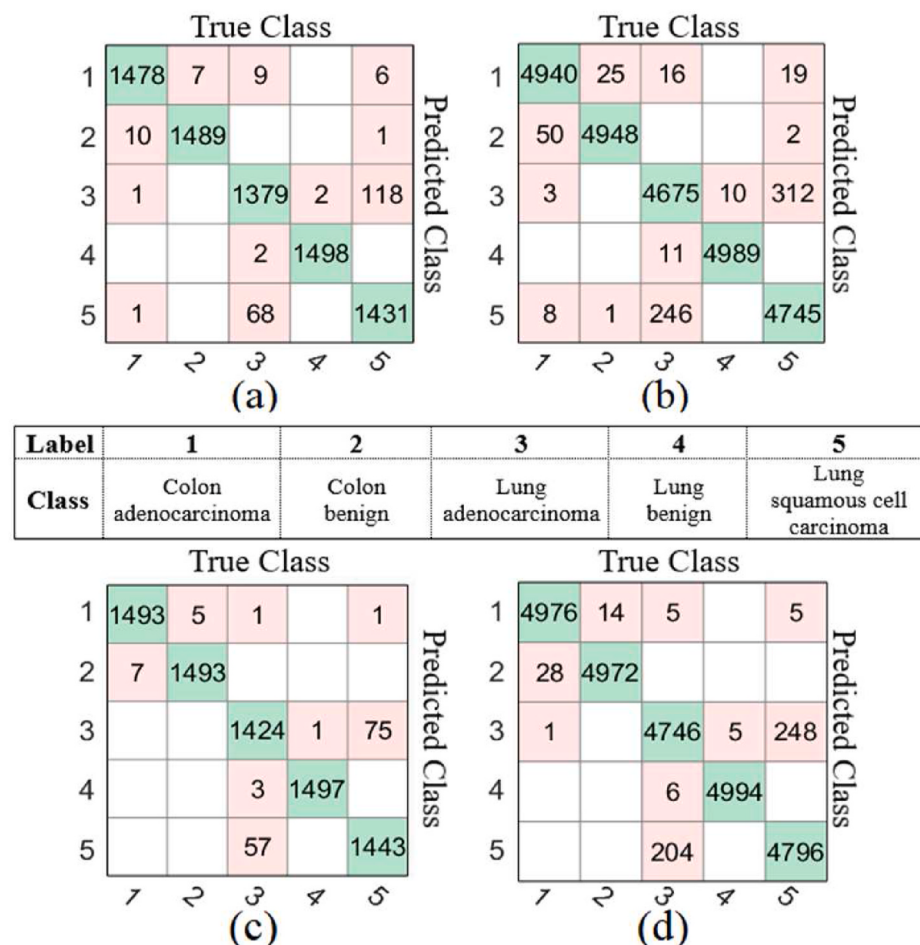


Fig. 8. The confusion matrices of the EO algorithm; (a) 30% test rate with inefficient feature set; (b) k fold value = 5 with inefficient feature set; (c) 30% test rate with efficient feature set; (d) k fold value = 5 with efficient feature set.

Table 5

Analysis results were obtained by the classification of the EO algorithm (inefficient features).

Class	Number Of Features	Test Rate	F-Scr. (%)	Se. (%)	Sp. (%)	Pre. (%)	Acc. (%)	Overall Acc. (%)
Colon adenocarcinoma	195	30%	98.86	98.53	99.79	99.19	99.53	97.0
Colon benign			99.39	99.26	99.87	99.53	99.75	
Lung adenocarcinoma			93.23	91.93	98.67	94.58	97.32	
Lung benign			99.86	99.86	99.96	99.86	99.94	
Lung squamous cell carcinoma			93.65	95.40	97.90	91.96	97.40	
Colon adenocarcinoma	k = 5	98.79	98.80	99.68	98.78	99.50		
Colon benign			99.21	98.96	99.86	99.47	99.68	
Lung adenocarcinoma			93.98	93.50	98.62	94.48	97.59	97.18
Lung benign			99.79	99.78	99.94	99.80	99.91	
Lung squamous cell carcinoma			94.16	94.90	98.32	93.44	97.63	

Table 6

Analysis results were obtained by the classification of the EO algorithm (efficient features).

Class	Number Of Features	Test ate	F-Scr. (%)	Se. (%)	Sp. (%)	Pre. (%)	Acc. (%)	Overall Acc. (%)
Colon adenocarcinoma	805	30%	99.53	99.53	99.88	99.53	99.80	98.0
Colon benign			99.59	99.53	99.91	99.66	99.83	
Lung adenocarcinoma			95.41	94.93	98.98	95.89	98.17	
Lung benign			99.86	99.80	99.98	99.93	99.94	
Lung squamous cell carcinoma			95.59	96.20	98.72	94.99	98.22	
Colon adenocarcinoma	k = 5	99.47	99.52	99.85	99.42	99.78		97.94
Colon benign			99.57	99.44	99.92	99.71	99.82	
Lung adenocarcinoma			95.29	94.92	98.92	95.66	98.12	
Lung benign			99.89	99.88	99.97	99.90	99.95	
Lung squamous cell carcinoma			95.45	95.92	98.73	94.98	98.16	

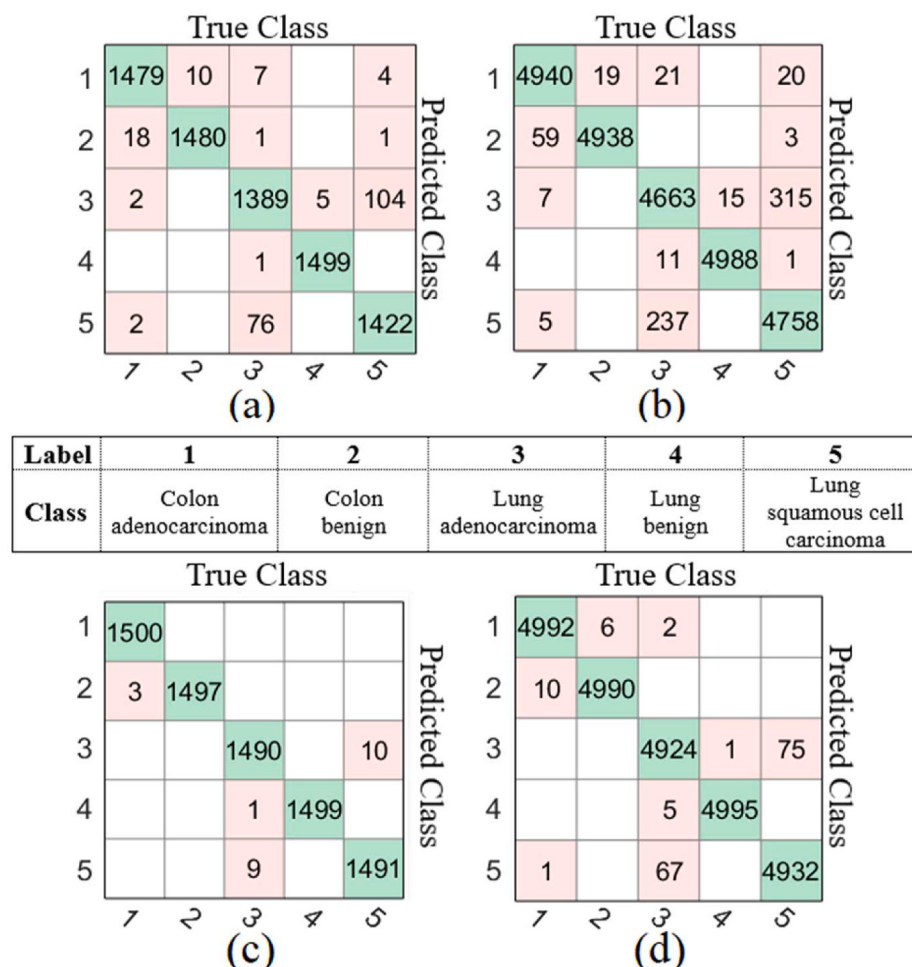


Fig. 9. Confusion matrices of dataset formed by combining the features obtained from MRFO and EO algorithm: (a) 30% test rate with inefficient feature set; (b) k fold value = 5 with inefficient feature set; (c) 30% test rate with the efficient feature set; (d) k fold value = 5 with the efficient feature set.

classified with SVM and the overall accuracy achieved was 96.92%. To verify the validity of this result, the feature set was reclassified by SVM with the cross-validation method, and the resulting classification overall accuracy rate was 97.14%. Afterward, a new dataset consisting of efficient features was obtained by separating the complementing rule in the set and the 1000-features dataset ($1000 - 270 = 730$ features). The 730 efficient feature dataset was classified with SVM and the overall accuracy achievement was 99.69%. To confirm the validity of this result, the dataset was separated by cross-validation ($k = 5$ fold) and reclassified by SVM. The overall accuracy success achieved with cross-validation was 99.33%. In this study, the proposed approach contributed to the classification of lung and colon cancer histopathological images. The confusion matrices of the third step are shown in Fig. 9. The results of the analysis obtained from the confusion matrices are given in Table 7 and Table 8 respectively.

In the last step of this experiment, the analyzes were performed using traditional feature selection methods. For this, F-regression [39], Lasso [40], Recursive Feature Elimination (RFE) [41], Ridge [42] feature selection methods were used. The set of 1000 features obtained from the Avg-1 layer of the DarkNet-19 model was processed with feature selection methods. These methods sorted the column numbers with all features according to efficiency, and by choosing the first 730 numbers, feature sets were created for each feature selection method. Then, the classification was carried out with the SVM method. The confusion matrices of the analyzes performed by the feature selection methods are shown in Fig. 10. The overall accuracy achievements obtained as a result of the analyzes are as follows: 95.41% success was achieved with f-regression, 96.25% success was achieved with Lasso, 96.03% success was achieved with RFE, and 95.76% success was achieved with Ridge. Analysis results are given in Table 9. Among the feature selection methods, the Lasso method gave the best performance. However, the overall accuracy achieved with the proposed approach was superior to the performance of feature selection methods.

4. Discussion

Cancer prevention is an important point in the fight against cancer, so early diagnosis is important in all types of cancer. However, accurate detection of cancer types and rapid results are seen by experts as a troublesome and lengthy process. To overcome these difficulties, it is necessary to follow the technological developments and involve them in the process. Each optimization algorithm may not show the initially determined target point or population with the best features each time it is run. This process may not always be effective for optimization algorithms. To make better use of metaheuristic optimization algorithms, it is necessary to consider the features that are out of the population during feature selection. In this study, it was observed that this approach gave successful results. The lack of a pre-processing step to reduce the noise of each image in the proposed approach or the fact that the proposed approach is not designed with an end-to-end approach can be shown among the limitations of this model.

Studies carried out by analyzing the dataset used in this study have

taken place in the literature. General information about the studies using the same dataset is given in Table 10.

Nishio et al. [43] performed the analyzes using three-class lung tissue images. They used the homology-based image processing technique and texture analysis technique as preprocessing steps. They used machine learning methods in the classification process. The overall accuracy they achieved in classification was 99.33%. It was observed that the preprocessing steps they used in their approach contributed to the experimental performance. But, they classified a three-class dataset. However, the overall success with the proposed approach outperformed their study.

Masud et al. [44] applied DFT and DWT algorithms as a pre-processing step to extract the feature from each image in the dataset. Then they trained the data with the CNN model they designed. They achieved an overall accuracy of 96.33% in the classification process they performed with Softmax. They observed that the DFT and DWT algorithms they used in the experimental analysis contributed to the achieved performance. However, they could have extracted the features from the last layer of the CNN model they designed (the layer with Softmax activation), and they could have trained these features with machine learning models. By doing so, perhaps their analysis could have improved the performance even more.

Wang et al. [45] designed a one-class learning-based Python package to detect tumor image types. They used the CNN model and the SVM method together in their proposed approach. The overall accuracy they achieved with the SVM model was 94%. Although the CNN model they used in their study was pre-trained, their success performance was lower than the analysis results of this study. Perhaps the redesign of the CNN model they designed could have contributed to the performance.

5. Conclusion

Cancer is an increasing disease all over the world in recent years, and there is an increase in mortality rates due to this disease [46]. According to various researches, lung and colon cancers, which have a low survival rate among cancer cases, have been presented in the first orders. Early diagnosis and treatment of cancer patients are important in this case [4, 47]. With this study, an artificial intelligence-supported approach that will contribute to early diagnosis using lung cancer and colon cancer images is proposed. With the proposed approach, a different perspective was brought to the metaheuristic optimization algorithms. As a result, an accuracy of 99.96% in colon adenocarcinoma data, 99.96% in colon benign data, 99.73% in lung adenocarcinoma data, 99.984% in lung benign data, and 99.74% in lung squamous cell carcinoma data was obtained. The overall accuracy rate of the proposed approach was 99.69%. With the approach proposed in this study, it has been observed that the used optimization algorithms contributed to the performance by applying the complementary rule in the set in the classification of cancer images.

In the future, it is planned to develop the proposed approach by using different structuring techniques that will contribute to the optimization algorithms, which will be different, for other datasets.

Table 7

Analysis results obtained of dataset formed by combining the features obtained from MRFO and EO algorithm (inefficient features).

Class	Number Of Features	Test Rate	F-Scr. (%)	Se. (%)	Sp. (%)	Pre. (%)	Acc. (%)	Overall Acc. (%)
Colon adenocarcinoma	270	30%	98.56	98.60	99.62	98.53	99.41	96.92
Colon benign			98.99	98.66	99.82	99.32	99.58	
Lung adenocarcinoma			93.40	92.60	98.57	94.23	97.37	
Lung benign			99.80	99.93	99.91	99.66	99.91	
Lung squamous cell carcinoma			93.83	94.80	98.16	92.88	97.49	
Colon adenocarcinoma		$k = 5$	98.69	98.80	99.63	98.58	99.46	
Colon benign			99.18	98.76	99.90	99.61	99.66	
Lung adenocarcinoma			93.89	93.26	98.64	94.54	97.56	97.14
Lung benign			99.73	99.76	99.92	99.70	99.88	
Lung squamous cell carcinoma			94.24	95.16	98.29	93.34	97.66	

Table 8

Analysis results obtained of dataset formed by combining the features obtained from MRFO and EO algorithm (efficient features).

Class	Number of Features	Test Rate	F-Scr. (%)	Se. (%)	Sp. (%)	Pre. (%)	Acc. (%)	Overall Acc. (%)
Colon adenocarcinoma	730	30%	99.90	100	99.94	99.80	99.96	99.69
Colon benign			99.89	99.80	100	100	99.96	
Lung adenocarcinoma			99.33	99.33	99.83	99.33	99.73	
Lung benign			99.96	99.93	100	100	99.98	
Lung squamous cell carcinoma			99.36	99.40	99.83	99.33	99.74	
Colon adenocarcinoma	k = 5	99.81	99.84	99.94	99.78	99.92	99.92	99.33
Colon benign		99.84	99.80	99.96	99.87	99.93		
Lung adenocarcinoma		98.49	98.48	99.62	98.51	99.40		
Lung benign		99.94	99.90	99.99	99.98	99.97		
Lung squamous cell carcinoma		98.57	98.64	99.62	98.50	99.42		

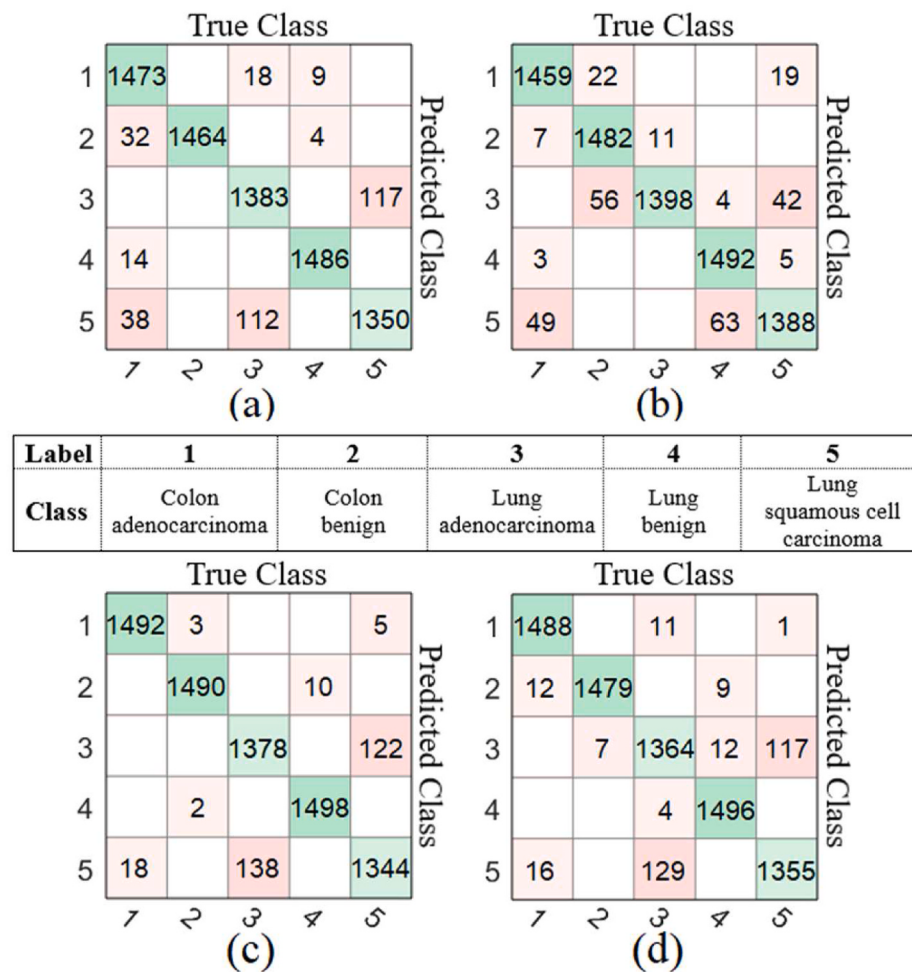


Fig. 10. Confusion matrices of feature selection methods: a) f-regression method, b) Lasso method, c) RFE method, d) Ridge method.

Table 9

Analysis results of traditional feature selection methods and the proposed method.

Method	Number of Features	Test Rate	Overall Accuracy (%)
f-regression	730	30%	95.41
Lasso			96.25
RFE			96.03
Ridge			95.76
Proposed Approach			99.69

Table 10

Comparison of other studies using the same dataset.

Article	Year	Model/Method	Overall Acc (%)
Nishio et al. [43]	2021	Feature extraction & Preprocessing & Machine learning	99.43
Masud et al. [44]	2021	Discrete Fourier Transform (DFT) & Discrete Wavelet Transform (DWT) & CNN	96.33
Wang et al. [45]	2021	CNN & SVM	94
Proposed Approach	2021	Deep learning & MRFO & EO	99.69

Funding

There is no funding source for this article.

Ethical approval

This article does not contain any data, or other information from studies or experimentation, with the involvement of human or animal subjects.

Declaration of competing interest

The author declares that there is no conflict of interest related to this paper.

References

- [1] A. Asuntha, A. Srinivasan, Deep learning for lung Cancer detection and classification, *Multimed. Tool. Appl.* 79 (2020) 7731–7762, <https://doi.org/10.1007/s11042-019-08394-3>.
- [2] L. Khairunnahar, M.A. Hasib, R.H. Bin Rezanur, M.R. Islam, M.K. Hosain, Classification of malignant and benign tissue with logistic regression, *Informatics Med. Unlocked*. 16 (2019), 100189, <https://doi.org/10.1016/j.imu.2019.100189>.
- [3] R.L. Siegel, K.D. Miller, A. Jemal, Cancer statistics, 2020, CA, *Cancer J. Clin.* 70 (2020) 7–30, <https://doi.org/10.3322/caac.21590>.
- [4] K. Kurishima, K. Miyazaki, H. Watanabe, T. Shiozawa, H. Ishikawa, H. Satoh, N. Hizawa, Lung cancer patients with synchronous colon cancer, *Mol. Clin. Oncol.* 8 (2018) 137–140, <https://doi.org/10.3892/mco.2017.1471>.
- [5] F. Demir, DeepCoroNet: a deep LSTM approach for automated detection of COVID-19 cases from chest X-ray images, *Appl. Soft Comput.* 103 (2021), 107160, <https://doi.org/10.1016/j.asoc.2021.107160>.
- [6] M. Turkoglu, COVIDetectioNet: COVID-19 diagnosis system based on X-ray images using features selected from pre-learned deep features ensemble, *Appl. Intell.* 51 (2021) 1213–1226, <https://doi.org/10.1007/s10489-020-01888-w>.
- [7] V. Tumen, O. Yildirim, B. Ergen, Recognition of road type and quality for advanced driver assistance systems with deep learning, *Elektron. Ir Elektrotehnika*. 24 (2018) 67–74, <https://doi.org/10.5755/j01.eie.24.6.22293>.
- [8] Y. Takahashi, K. Sone, K. Noda, K. Yoshida, Y. Toyohara, K. Kato, F. Inoue, A. Kukita, A. Taguchi, H. Nishida, Y. Miyamoto, M. Tanikawa, T. Tsuruga, T. Iriyama, K. Nagasaka, Y. Matsumoto, Y. Hirota, O. Hiraike-Wada, K. Oda, M. Maruyama, Y. Osuga, T. Fujii, Automated system for diagnosing endometrial cancer by adopting deep-learning technology in hysteroscopy, *PloS One* 16 (2021), e0248526, <https://doi.org/10.1371/journal.pone.0248526>.
- [9] S. Wang, T. Wang, L. Yang, D.M. Yang, J. Fujimoto, F. Yi, X. Luo, Y. Yang, B. Yao, S. Lin, C. Moran, N. Kalhor, A. Weissferdt, J. Minna, Y. Xie, I.I. Wistuba, Y. Mao, G. Xiao, ConvPath: a software tool for lung adenocarcinoma digital pathological image analysis aided by a convolutional neural network, *EBioMedicine* 50 (2019) 103–110, <https://doi.org/10.1016/j.ebiom.2019.10.033>.
- [10] A. Teramoto, T. Tsukamoto, Y. Kiriya, H. Fujita, Automated classification of lung cancer types from cytological images using deep convolutional neural networks, *BioMed Res. Int.* 2017 (2017), 4067832, <https://doi.org/10.1155/2017/4067832>.
- [11] J.W. Wei, L.J. Tafe, Y.A. Linnik, L.J. Vaickus, N. Tomita, S. Hassannpour, Pathologist-level classification of histologic patterns on resected lung adenocarcinoma slides with deep neural networks, *Sci. Rep.* 9 (2019) 3358, <https://doi.org/10.1038/s41598-019-40041-7>.
- [12] M. Shapcott, K.J. Hewitt, N. Rajpoot, Deep learning with sampling in colon cancer histology, *Front. Bioeng. Biotechnol.* 7 (2019) 52, <https://doi.org/10.3389/fbio.2019.00052>.
- [13] N. Gessert, M. Bengs, L. Wittig, D. Drömann, T. Keck, A. Schlaefer, D.B. Ellebrecht, Deep transfer learning methods for colon cancer classification in confocal laser microscopy images, *Int. J. Comput. Assist. Radiol. Surg.* 14 (2019) 1837–1845, <https://doi.org/10.1007/s11548-019-02004-1>.
- [14] T.L.T. Vuong, D. Lee, J.T. Kwak, K. Kim, Multi-task deep learning for colon cancer grading, *Int. Conf. Electron. Information. Commun.* 2020 (2020) 1–2, <https://doi.org/10.1109/iceic49074.2020.9051305>.
- [15] B. Hur, D. Kang, S. Lee, J.H. Moon, G. Lee, S. Kim, Venn-diaNet: venn diagram based network propagation analysis framework for comparing multiple biological experiments, *BMC Bioinf.* 20 (2019) 1–12, <https://doi.org/10.1186/s12859-019-3302-7>.
- [16] M. Attenborough, 4 - Boolean Algebra, in: M.B.T.-M. for E.E, C. Attenborough (Eds.), Newnes, Oxford, 2003, pp. 76–87, <https://doi.org/10.1016/B978-075065855-3/50030-9>.
- [17] A.A. Borkowski, M.M. Bui, L.B. Thomas, C.P. Wilson, L.A. DeLand, S.M. Mastorides, Lung and colon cancer histopathological image dataset (LC25000), ArXiv Prepr. ArXiv1912.12142 (2019) 1–2, <https://arxiv.org/abs/1912.12142v1>.
- [18] Andrew A. Borkowski, Marilyn M. Bui, L. Brannon Thomas, Catherine P. Wilson, Lauren A. DeLand, Stephen M. Mastorides, Lung and Colon Cancer Histopathological Images Dataset, Kaggle, 2021. <https://www.kaggle.com/andrewmvd/lung-and-colon-cancer-histopathological-images>. (Accessed 21 August 2021).
- [19] J. Redmon, A. Farhadi, YOLO9000: better, faster, stronger, proc. - 30th IEEE conf. Comput. Vis. Pattern recognition. CVPR 2017. 2017-Janua, 2017, pp. 6517–6525, <https://doi.org/10.1109/cvpr.2017.690>.
- [20] F. Demir, A.M. Ismael, A. Sengur, Classification of lung sounds with CNN model using parallel pooling structure, *IEEE Access* 8 (2020) 105376–105383, <https://doi.org/10.1109/ACCESS.2020.3000111>.
- [21] T. Ozturk, M. Talo, E.A. Yildirim, U.B. Baloglu, O. Yildirim, U. Rajendra Acharya, Automated detection of COVID-19 cases using deep neural networks with X-ray images, *Comput. Biol. Med.* 121 (2020), 103792, <https://doi.org/10.1016/j.combiomed.2020.103792>.
- [22] M. Awad, R. Khanna, Support Vector Machines for Classification BT - Efficient Learning Machines: Theories, Concepts, and Applications for Engineers and System Designers, in: M. Awad, R. Khanna (Eds.), Apress, Berkeley, CA, 2015, pp. 39–66, https://doi.org/10.1007/978-1-4302-5990-9_3.
- [23] E. Başaran, Z. Cömert, A. Şengür, Ü. Budak, Y. Çelik, M. Toğacar, Chronic Tympanic Membrane Diagnosis Based on Deep Convolutional Neural Network, in: 2019 4th Int. Conf. Comput. Sci. Eng., 2019, pp. 1–4, <https://doi.org/10.1109/ubmk.2019.8907070>.
- [24] M. Loey, G. Manogaran, M.H.N. Taha, N.E.M. Khalifa, A hybrid deep transfer learning model with machine learning methods for face mask detection in the era of the COVID-19 pandemic, *Meas. J. Int. Meas. Confed.* 167 (2021), 108288, <https://doi.org/10.1016/j.measurement.2020.108288>.
- [25] S. Huang, N. Cai, P.P. Pacheco, S. Narrandes, Y. Wang, W. Xu, Applications of Support vector machine (SVM) learning in cancer genomics, *Cancer Genomics Proteomics* 15 (2017) 41–51, <https://doi.org/10.21873/cgp.20063>.
- [26] G.N. Kouziokas, SVM kernel based on particle swarm optimized vector and Bayesian optimized SVM in atmospheric particulate matter forecasting, *Appl. Soft Comput.* 93 (2020), 106410, <https://doi.org/10.1016/j.asoc.2020.106410>.
- [27] W. Zhao, Z. Zhang, L. Wang, Manta ray foraging optimization: an effective bio-inspired optimizer for engineering applications, *Eng. Appl. Artif. Intell.* 87 (2020), 103300, <https://doi.org/10.1016/j.engappai.2019.103300>.
- [28] S.I. Selem, H.M. Hasanien, A.A. El-Fergany, Parameters extraction of PEMFC's model using manta rays foraging optimizer, *Int. J. Energy Res.* 44 (2020) 4629–4640, <https://doi.org/10.1002/er.5244>.
- [29] E.H. Houssein, M.M. Eman, A.A. Ali, Improved manta ray foraging optimization for multi-level thresholding using COVID-19 CT images, *Neural Comput. Appl.* (2021), <https://doi.org/10.1007/s00521-021-06273-3>.
- [30] O.E. Turgut, A novel chaotic manta-ray foraging optimization algorithm for thermo-economic design optimization of an air-fin cooler, *SN Appl. Sci.* 3 (2020) 3, <https://doi.org/10.1007/s42452-020-04013-1>.
- [31] A. Faramarzi, M. Heidarinejad, B. Stephens, S. Mirjalili, Equilibrium optimizer: a novel optimization algorithm, *Knowl. Base Syst.* 191 (2020), 105190, <https://doi.org/10.1016/j.knosys.2019.105190>.
- [32] H. Chen, P.C. Boutros, VennDiagram: a package for the generation of highly-customizable Venn and Euler diagrams in R, *BMC Bioinf.* 12 (2011) 35, <https://doi.org/10.1186/1471-2105-12-35>.
- [33] F. Sheridan, A variant of Church's set theory with a universal set in which the singleton function is a set, *Log. Anal.* 59 (2016) 81–131, <https://doi.org/10.2143/LEA.23.0.3149532>.
- [34] K.K. Ghosh, Metaheuristic Optimization: Different Meta-Heuristic Optimization Techniques for Feature Selection, Github, 2021. <https://github.com/Rangerix/MetahuristicOptimization>. (Accessed 10 June 2021).
- [35] J. Kim, T.A.H. Kim, W.J. Song, Architecture-level simulation framework for neural network acceleration hardware, *Sch. Electr. Electron. Eng. Yonsei Univ.* 2 (2019). https://icsl.yonsei.ac.kr/wp-content/uploads/eee4610_spring2018-2.pdf.
- [36] S. Sayyad, M. Shaikh, A. Pandit, D. Sonawane, S. Anpat, Confusion Matrix-Based Supervised Classification Using Microwave SIR-C SAR Satellite Dataset BT - Recent Trends in Image Processing and Pattern Recognition, in: K.C. Santosh, B. Gawali (Eds.), Springer Singapore, Singapore, 2021, pp. 176–187.
- [37] F. Demir, A. Sengur, V. Bajaj, Convolutional neural networks based efficient approach for classification of lung diseases, *Health Inf. Sci. Syst.* 8 (2019) 4, <https://doi.org/10.1007/s13755-019-0091-3>.
- [38] F. Rahmad, Y. Suryanto, K. Ramlil, Performance comparison of anti-spam technology using confusion matrix classification, *IOP Conf. Ser. Mater. Sci. Eng.* 879 (2020), 12076, <https://doi.org/10.1088/1757-899x/879/1/012076>.
- [39] M. Toğacar, B. Ergen, Z. Cömert, Classification of flower species by using features extracted from the intersection of feature selection methods in convolutional neural network models, *Measurement* 158 (2020), 107703, <https://doi.org/10.1016/j.measurement.2020.107703>.
- [40] L. Jiang, C.M.T. Greenwood, W. Yao, L. Li, Bayesian hyper-LASSO classification for feature selection with application to endometrial cancer RNA-seq data, *Sci. Rep.* 10 (2020) 9747, <https://doi.org/10.1038/s41598-020-66466-z>.
- [41] H. Jeon, S. Oh, Hybrid-recursive feature elimination for efficient feature selection, *Appl. Sci.* 10 (2020) 3211, <https://doi.org/10.3390/app10093211>.
- [42] M. Toğacar, B. Ergen, Z. Cömert, Classification of white blood cells using deep features obtained from Convolutional Neural Network models based on the combination of feature selection methods, *Appl. Soft Comput.* 97 (2020), 106810, <https://doi.org/10.1016/j.asoc.2020.106810>.
- [43] M. Nishio, M. Nishio, N. Jimbo, K. Nakane, Homology-based image processing for automatic classification of histopathological images of lung tissue, *Cancers* 13 (2021) 1192, <https://doi.org/10.3390/cancers13061192>.
- [44] M. Masud, N. Sikder, A.-A. Nahid, A.K. Bairagi, M.A. AlZain, A machine learning approach to diagnosing lung and colon cancer using a deep learning-based classification framework, *Sensors* 21 (2021) 748, <https://doi.org/10.3390/s21030748>.

- [45] Y. Wang, L. Yang, G.I. Webb, Z. Ge, J. Song, OCTID: a one-class learning-based Python package for tumor image detection, *Bioinformatics* (2021), <https://doi.org/10.1093/bioinformatics/btab416>.
- [46] D. Cinar, D. Tas, Cancer in the elderly, north, *Clin. Istanbul.* 2 (2015) 73–80, <https://doi.org/10.14744/nci.2015.72691>.
- [47] P. Rawla, T. Sunkara, A. Barsouk, Epidemiology of colorectal cancer: incidence, mortality, survival, and risk factors, *Przeglad Gastroenterol.* 14 (2019) 89–103, <https://doi.org/10.5114/pg.2018.81072>.